
Biodegradable fumarate-based drug-delivery systems for ophthalmic applications

M. C. Hacker,^{1*} A. Haesslein,^{1*} H. Ueda,^{1†} W. J. Foster,^{2,3} C. A. Garcia,⁴ D. M. Ammon,⁵ R. N. Borazjani,⁵ J. F. Kunzler,⁵ J. C. Salamone,⁵ A. G. Mikos¹

¹Department of Bioengineering, Rice University, MS-142, P.O. Box 1892, Houston, Texas 77251-1892

²Department of Physics, The University of Houston, Houston, Texas 77204-5005

³Department of Ophthalmology, Weill Medical College of Cornell University at The Methodist Hospital, Houston, Texas 77030

⁴Department of Ophthalmology and Visual Sciences, The University of Texas, Houston School of Medicine, Houston, Texas 77030

⁵Bausch and Lomb Vision Care, Rochester, New York 14603-0450

Received 15 November 2007; revised 10 December 2007; accepted 11 December 2007

Published online 2 April 2008 in Wiley InterScience (www.interscience.wiley.com). DOI: 10.1002/jbm.a.31942

Abstract: The function of a photocrosslinked poly(propylene fumarate) (PPF)/poly(*N*-vinyl pyrrolidone) (PVP) matrix for the sustained release of three ophthalmic model drugs, acetazolamide (AZ), dichlorphenamide (DP), and timolol maleate (TM), was investigated. The drugs differ in molecular weight and degree of dissociation in aqueous environments; both are parameters that significantly influence drug diffusivity. AZ, DP, and TM-loaded cylindrical rods (10 mm length, 0.6 mm diameter) were fabricated by photoinduced cross-copolymerization of PPF and *N*-vinyl pyrrolidone (NVP) in molds. The released amounts of AZ, DP, TM, and NVP were determined by high-performance liquid chromatography (HPLC). The effects of drug properties and loading on the release kinetics were investigated. The *in vitro* release of AZ, DP, and TM was well sustained from the polymer matrices over a period of ~210, 270, and 250 days, respectively. The release kinetics correlated with the HPLC retention profiles of the different drugs. Follow-

ing a small initial burst release (<10%), a dual modality release controlled by diffusion and bulk erosion was found for all drugs. Drug release rates of up to 4 µg/day were reached. Matrix drug loading generally affected the extent of the burst release, release kinetics, as well as the matrix water content and matrix degradation that were determined gravimetrically. Microcomputed tomography was used to image structural and dimensional changes of the devices. A preliminary rabbit implantation study revealed promising ocular biocompatibility of drug-free PPF/PVP matrices. All results indicate the potential of photocrosslinked PPF-based matrices as polymeric carriers for long-term ophthalmic drug delivery. © 2008 Wiley Periodicals, Inc. *J Biomed Mater Res* 88A: 976–989, 2009

Key words: acetazolamide; dichlorphenamide; timolol maleate; intraocular drug delivery; biodegradable polymer implant; poly(propylene fumarate)

INTRODUCTION

Systemic drug application has been shown to be inefficient in the treatment of several chronic disorders of internal structures of the eye due to the bio-

physiologic blood-ocular barriers.^{1–3} Different strategies for the direct delivery of therapeutic agents to the anterior or posterior segment of the eye have therefore been investigated. For the latter, these strategies include intraocular drug injection and the use of polymeric drug-delivery systems.^{2,4} Sustained drug delivery to the eye is critical for the safe and successful treatment of degenerative diseases that are associated with severe vision loss. These disorders include age-related macular degeneration, diabetic retinopathy, glaucoma, and retinitis pigmentosa.⁵ Repeated intraocular injections remain the delivery route of choice in many therapeutic approaches to address these disorders. Frequent injections, however, are often of poor compliance, and they can pose significant risk, including retinal detachment, endophthalmitis, and formation of cataracts. Biodegradable and nondegradable drug-polymer matrices for implantation or

*These authors contributed equally to this work.

†Present address: Department of Biomaterials, Field of Tissue Engineering, Institute for Frontier Medical Sciences, Kyoto University, 53 Kawara-cho Shogoin, Sakyo-ku, Kyoto 606-8507, Japan

Correspondence to: A. G. Mikos; e-mail: mikos@rice.edu

Contract grant sponsors: Bausch & Lomb, Rochester, NY, Japanese Science Foundation Postdoctoral Fellowship

Contract grant sponsor: Deutsche Forschungsgemeinschaft (DFG); contract grant number: HA4444-1/1

Contract grant sponsor: National Eye Institute of the National Institutes of Health

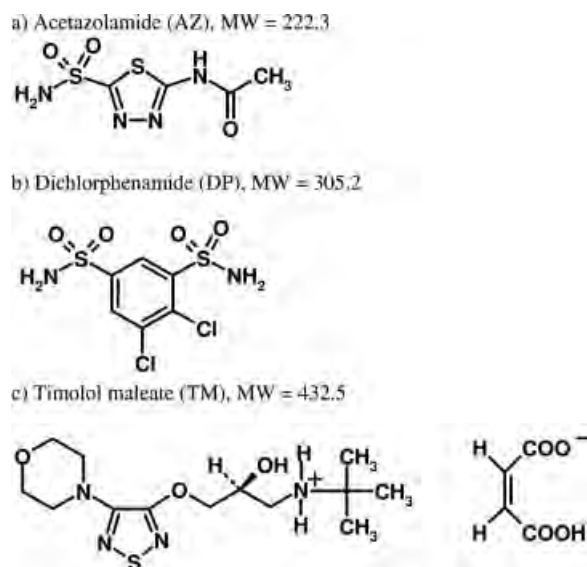


Figure 1. Chemical structures and molecular weights (MW) of the investigated ophthalmic model drugs. (a) Acetazolamide (AZ), (b) dichlorophenamide (DP), and (c) timolol maleate (TM).

injection have been explored for the localized long-term delivery of ophthalmic drugs to the posterior eye.⁴ In our laboratory, we have recently described the potential application of photocrosslinked poly(propylene fumarate) (PPF)-based implants for the long-term delivery of the antiinflammatory corticosteroid fluocinolone acetonide (FA).⁶ The matrices, which were composed of the biodegradable, crosslinkable polyester PPF and *N*-vinyl pyrrolidone (NVP), controlled the release of FA over a 1-year period. A subsequent study investigated drug release from injectable PPF implants with and without additional surface crosslinking and showed that FA release was sustained over a comparable period.⁷ The burst release, however, was significantly higher from the injectable systems when compared with the pre-fabricated implants. In view of the promising long-term release profiles that were found for FA from the photocrosslinked networks, this study investigated the release profiles of other ophthalmic drugs from PPF-based implants. Two carbonic anhydrase inhibitors, acetazolamide (AZ) and dichlorophenamide (DP), and the β -adrenoreceptor antagonist timolol maleate (TM) were selected as model ophthalmic drugs, because they are effectively used as glaucoma therapeutics (Fig. 1).^{8–10} Very limited information is available on the transscleral or intravitreal delivery of antiglaucoma drugs.^{11,12} Normally, these drugs are applied topically, and research is focused on improving transcorneal penetration because therapeutic levels have to be reached in the aqueous humor and at the iris/ciliary body. In general, there is a concern about the systemic side effects of antiglaucoma drugs, which, in part, may result due to drug resorption

from the posterior chamber.¹³ AZ, however, is commonly applied systemically because of the drug's poor transcorneal bioavailability.⁸ The characteristic chemical functionalities of antiglaucoma drugs often cause these drugs to dissociate in physiological environments and promote good water solubility. Because of these physicochemical properties, antiglaucoma drugs are interesting model drugs for the testing of polymeric ocular drug-delivery systems as drug properties differ significantly from commonly delivered drugs such as corticosteroids and antiviral drugs.¹¹ Through the use of these more hydrophilic model drugs (AZ, DP, and TM), effects of drug properties on drug release can be obtained in comparison to the lipophilic corticosteroid FA, which was investigated in a previous study.⁶ As a result of the structural differences, the partition equilibria of the drugs between aqueous solution and hydrophobic polymer bulk differ significantly, and corresponding diffusion coefficients are expected to be significantly increased.

The aim of this work was to investigate the *in vitro* release profiles of the model ophthalmic drugs AZ, DP, and TM from the photocrosslinked PPF-based matrices and to correlate the observed release kinetics to the drug properties. The drugs were embedded in monolithic matrices composed of PPF and NVP of a previously established composition.⁶ *In vitro* release of AZ, DP, and TM was investigated for different drug loadings over periods up to 300 days. Quantification of released drug molecules and NVP monomers was done using high-performance liquid chromatography (HPLC). Because adsorption-desorption phenomena determine substance retention in liquid chromatography and similar mechanisms control drug diffusion in polymer matrices, the drugs' retention profiles on a reversed-phase HPLC column were compared and used as a means to compare the drugs' partition equilibria, which are controlled by molecular weight (MW) and drug dissociation. Matrix water content and degradation were analyzed gravimetrically. Microcomputed tomography (micro-CT) was used to quantify structural and dimensional changes of the drug-delivery systems. A preliminary 2-week rabbit implantation study was conducted to obtain initial biocompatibility data for plain polymer matrices.

MATERIALS AND METHODS

Materials

AZ, DP, and TM were purchased from Sigma-Aldrich (Milwaukee, WI). Diethyl fumarate, 1-vinyl-2-pyrrolidone (NVP) (both from Sigma-Aldrich), propylene glycol (Fisher, Pittsburgh, PA), zinc chloride (Acros, Pittsburgh, PA), and bis(2,4,6-trimethylbenzoyl) phenylphosphine oxide (BAPO) (kindly provided by Ciba Specialty Chemicals, Tarrytown,

TABLE I
Composition of Drug-Loaded, Photocrosslinked Poly(propylene fumarate)/poly(*N*-vinyl pyrrolidone) (PPF/PVP) Matrices Investigated for the *In Vitro* Release of Acetazolamide (AZ), Dichlorphenamide (DP), and Timolol Maleate (TM)

Sample Code	AZ 2.5%	AZ 5%	DP 5%	DP 10%	TM 5%
Matrix Composition PPF:NVP (w/w)			3:2		3:2
PPF Macromer (M_n , M_w) [Da]		2000 ± 10, 4080 ± 70			2050 ± 10, 3170 ± 40
Drug	AZ			DP	TM
Loading [% (w/w)]	2.5	5.0	5.0	10.0	5.0

Molecular weight data for PPF as obtained by gel permeation chromatography.

NY) were used as received. Phosphate buffered saline (PBS) was obtained from Gibco (Grand Island, NY). All chemical solvents were of analytical quality and purchased from Fisher.

Transparent RTV (room temperature vulcanization) silicone rubber molds were fabricated following the manufacturer's instructions (Silicones, High Point, NC). Briefly, a two-component silicone mixture was poured over a Nickel-Chrome wire (diameter: 0.6 mm) in a petri dish and allowed to cure for 24 h. The rubber was trimmed, and the wire was removed with a scalpel to form a one-part mold with two injection ports.¹⁴ The silicone molds were stored under vacuum and purged with nitrogen gas before their use for implant fabrication.

Methods

Synthesis of poly(propylene fumarate)

Poly(propylene fumarate) (PPF) was synthesized in a two-step reaction process as described previously.¹⁵ Bis(2-hydroxypropyl) fumarate was synthesized from 1 mol of diethyl fumarate with 3 mol of propylene glycol through ZnCl₂-catalyzed transesterification and subsequently polymerized by transesterification and continuous removal of evolved propylene glycol at low pressure (<3 mmHg) to form PPF. The reaction was run until the desired number-average molecular weight (M_n) was obtained. After different washing and extraction steps, volatiles were removed by rotoevaporation and vacuum drying. MW characterization of purified PPF was done by gel permeation chromatography on a Styragel HR2 column (Waters, Milford, MA) relative to poly(styrene) standards (Waters). PPF (M_n = 2000 ± 10 Da, M_w = 4080 ± 70 Da) was used for the fabrication of AZ and DP-loaded matrices. TM-loaded implants consisted of PPF characterized by an M_n of 2050 ± 10 Da and an M_w of 3170 ± 40 Da (Table I).

Fabrication of drug-loaded PPF/PVP drug-delivery systems

Monolithic, nonporous polymer matrices loaded with AZ, DP, and TM were fabricated as described in a previous publication.⁶ Table I summarizes the investigated matrix compositions. In short, the precisely measured amount of drug was dissolved in the appropriate amount of NVP. The resulting solution was then mixed with the required amount of PPF.

Finally, 0.5% (w/w) of the photoinitiator BAPO was added as acetic solution (100 mg/mL), and the components were thoroughly mixed. Using a syringe equipped with a 22-gauge needle, the mixture was injected into a silicone mold. Once the cavity (inner diameter: 0.6 mm) was filled, the mold was placed under a blue curing light (3M Dental Products, St. Paul, MN) for 10 min to crosslink the matrix.¹⁶ The distance between light guide and mold was 8 cm. The blue light source, which contains a 75-W halogen bulb, is specified to emit visible light limited to the range of 400–500 nm with a peak irradiance of 14 mW/cm² at 470 nm.

Before the *in vitro* release study, the cylindrical cross-linked PPF/poly(*N*-vinyl pyrrolidone) (PVP) matrices were cut into rods of 10 mm length (diameter: 0.6 mm, typical weight: 3.8 mg). A drug loading of 2.5% (w/w) and 5% (w/w) was tested for AZ. DP-loaded matrices contained 5% and 10% (w/w) of the drug. These drug loadings were selected based on the maximum amounts of drug soluble in NVP, tested in 2.5% increments, and the corresponding 50% values. Accordingly, higher concentrations of DP were soluble in NVP when compared to AZ. For TM, a single drug loading of 5% (w/w) was investigated in this study (Table I).

In vitro release of AZ, DP, and TM from the PPF/PVP matrices

To determine the *in vitro* release kinetics, drug-loaded polymer rods were submerged and maintained in 2 mL of PBS (pH 7.4) in glass vials at 37°C with agitation (~75 rpm). At predetermined time points (6 h, 12 h, 1 d, 2 d, 3 d, 5 d, 7 d, and weekly afterward), the supernatant was collected, replaced with fresh PBS, and stored at 2–8°C until analysis. HPLC was used to quantify the amounts of released drug and NVP monomers. The *in vitro* study was stopped when no drug release was detectable from all three samples of one formulation at three consecutive time points.

The amount of drug released during the first day of the experiment was reported as the burst release. After day 1, drug release rates were determined from the amount of drug (microgram) released between two consecutive data points divided by the corresponding release time (typically: 7 days) and are thus expressed as microgram drug per day.

High-performance liquid chromatography analysis

A high-performance liquid chromatography (HPLC) system consisting of a Waters Alliance 2695XE separation

TABLE II
Chromatographic Conditions as Applied for Analysis of the *In Vitro* Release Samples

Drug	Column(s)	Acidic Buffer—A	Organic Phase—B	Mix A:B (v/v)	Retention Time (min)	
					Drug	NVP
AZ	ZORBAX SB-C8 (guard) ZORBAX 300SB-C8	Sodium acetate, 0.4M, pH 4.85	Acetonitrile	92.5:7.5	1.3	3.7
DP	ZORBAX 300SB-CN	Sodium acetate, 0.4M, pH 4.85	Acetonitrile	95:5	0.6	3.4
TM	XTerra [®] MS C18 (guard) XTerra [®] RP18	Sodium phosphate, 0.2M, pH 2.8	Methanol	77.5:22.5	5.8	2.1

The retention times of the different drugs and NVP were calculated as the differences between the elution times of the substances and the injection signals.

module and a Waters 2996 photodiode array detector (Waters) was used to determine the amount of released drugs and NVP monomers. In a typical run, 50 μ L of the collected supernatant was injected and analyzed on a reversed-phase column thermostated at 30°C. Reversed-phase columns in combination with isocratic mixtures of acidic buffers and acetonitrile or methanol were used as mobile phases at a flow rate of 1 mL/min. The chromatographic conditions were optimized to meet the following criteria: (1) achieve run times as short as 10 min and (2) generate sufficient separation between injection peak, drug signal, and NVP peak. The chromatographic conditions developed for the different drugs are summarized in Table II. Quantification was done by UV spectrophotometric detection at wavelengths of 265 nm (AZ), 232 nm (DP), 295 nm (TM), and 235 nm (NVP). Calibration standards were prepared from stock solutions of the different drugs (AZ: 0.5 mg/mL in ethanol, DP: 1 mg/mL in acetonitrile, and TM: 1 mg/mL in PBS) and NVP (1 mg/mL in PBS) by dilution with PBS. For each substance, the concentration of the different standard dilutions was proportional to the integrated area of the corresponding peak in UV absorbance. The calibration curves were linear ($R^2 > 0.999$) over the recorded concentration range (drugs: 0.025–100 μ g/mL; NVP: 0.5–25 nL/mL).

Comparison of drug partition profiles by reversed-phase HPLC

The partition coefficient ($\log P$), which describes the partition of nondissociated molecules between a hydrophilic (typically water) and a hydrophobic phase (typically 1-octanol), is known to correlate with the diffusion coefficient of a substance in a hydrophobic matrix. HPLC can be used to determine the partition coefficient of a substance because partition coefficient and retention volume on a reversed-phase column of a specific substance are in direct proportion.^{17,18} Absolute $\log P$ values can be determined through linear regression by correlating retention time (RT) with RTs of similar compounds for which the partition coefficients are known. In view of the dissociation of the investigated drugs in physiological media and the lack of suitable reference substances, the determination of the absolute partition coefficients was not attempted. A relative comparison, however, that aims at determining interactions between the

dissociated drugs and a hydrophobic polymer surface at 37°C, was performed on a reversed-phase C8 column. Ideally, one would use a chromatographic setup that uses a C18 reversed-phase column in combination with PBS as the mobile phase. Such a setup, however, proved unsuitable for a comparison between the drugs AZ, DP, TM, and FA, because FA was not eluted from the hydrophobic C18 column within 3 h (data not shown). FA was included in these experiments to enable comparisons between all ophthalmic drugs that were released from PPF/PVP matrices in the present and in a previous study.⁶ Also, with regard to suitable elution times, a 90:10 (v/v) mixture of PBS and acetonitrile was used as the mobile phase. Specifically, solutions of AZ, DP, TM, and FA (all 0.1 mg/mL) in PBS were analyzed individually and as a mixture containing equal amounts of all four solutions on the Waters HPLC system described earlier. A 50- μ L sample was injected and separated on a ZORBAX 300SB-C8 5 μ m column (4.6 \times 150 mm) combined with a ZORBAX SB-C8 Guard 5 μ m (4.6 \times 12.5 mm) guard column using a 90:10 (v/v) mixture of PBS and acetonitrile as the mobile phase at a flow rate of 1 mL/min. The system was thermostated at 37°C to simulate conditions relevant for comparison with the *in vitro* release experiments. Over a run time of 180 min, UV absorption was recorded at wavelengths of 265 nm (AZ), 232 nm (DP), 295 nm (TM), and 238 nm (FA). Absolute RTs of the different drugs were calculated as the difference in RT between drug molecule and injection signal. No significant differences were observed between the RTs obtained from the individual runs and the chromatograms of the drug mixture.

Gravimetric analysis

Before the *in vitro* release study, the initial dry weight of the samples was determined on an analytical balance (AX105 Delta Range, Mettler-Toledo, Columbus, OH). After completion of the release study (t_{end}), samples were removed from the release buffer, patted gently with a tissue paper, and subsequently weighed to determine the wet weights of the samples. The final dry weights of the samples were obtained after lyophilization (FreeZone 4.5 Liter Console, Freeze Dry Systems, Kansas City, MO) for 48 h. The relative sample water uptake was calculated from the difference between the wet and final dry weight relative to the sample's final dry weight. Relative weight loss was cal-

TABLE III
Implantation Plan and Sample Codes of Rabbit Implantation Study

Rabbit	1		2		3		4	
Eye (Left/Right)	L	R	L	R	L	R	L	R
Site (Sclera/Vitreous)	S	V	S	V	S	V	S	V
BaSO ₄ (+/-)	-	-	+	+	+	+	-	-
Code (Rabbit, Site, BaSO ₄)	1S-	1V-	2S+	2V+	3S+	3V+	4S-	4V-

culated as the difference between the final and initial dry weights relative to the sample's initial weight. Matrix loss was calculated by subtracting the amount of released drug and NVP monomers, as determined by HPLC, from the absolute weight loss of each sample. Matrix loss was expressed relative to the sample's initial weight.

Structural sample analysis

In vitro release study

Nondestructive dimensional analysis of the samples was performed by means of a micro-CT system without the use of a contrast agent (Desktop Micro CT1172, SkyScan, Aartselaar, Belgium). Each sample was fixed vertically to the scan plane on a sample holder (height 4.5 cm, width 0.4 cm) and scanned at a resolution of 3.1 μm , with a source voltage of 40 kV and a current of 250 μA . X-ray radiographs were recorded at different angles during step-wise rotation (step size: 0.7°) of the samples between 0° and 180°. After image acquisition, the scans were analyzed using the SkyScan software package provided with the instrument. The serial slices (2-D transverse cross-sections) of the rods were reconstructed with SkyScan reconstruction software. The areas of the scanned and reconstructed cross sections (over a length of 1.5 mm which equals 577 sections) were calculated using the standard SkyScan software (CTAn). Samples were scanned and quantified after fabrication and after lyophilization subsequent to completion of the *in vitro* release study. From the obtained data sets, the changes in cross-sectional area were calculated.

In vivo implantation study.

Half of the implanted matrices were loaded with 5% (w/w) barium sulfate to enhance radiopacity of the samples (Table III). Explanted samples were analyzed by micro-CT, and the results were compared to the data gathered before implantation to determine changes in cross-sectional area and porosity as measures of implant erosion. As the intrascleral samples were retrieved together with surrounding tissue, the entire specimens were rehydrated in purified water for 1 h after fixation and tightly wrapped in Parafilm[®] to avoid shrinking during the scanning time. The explants that had been placed intravitreally were scanned after washing and lyophilization. The specimens were scanned at a resolution of 3.1 μm and 7.0 μm for the implants that had been placed intravitreally and intrasclerally, respectively.

Rabbit implantation study

To evaluate the tissue response to plain PPF/PVP matrices, a preliminary *in vivo* implantation study was performed on 4-month-old female New Zealand albino rabbits. This study was performed in compliance with the U.S. National Institutes of Health Guidelines for the Care and Use of Laboratory Animals and the ethical use protocols (IACUC) of Rice University. The episclera and the vitreous body were tested as application sites. None of the PPF/PVP samples contained drugs. Half of the tested matrices were loaded with barium sulfate (5% (w/w)) (Sigma-Aldrich) to increase the radiopacity of the implants during micro-CT imaging. A 7-cm-long suture thread (Prolene 6-0, Ethicon, Sommerville, NJ) was embedded at one end of each implant during the photocrosslinking step to ensure a stable anchoring of the implant in the appropriate position. With regard to the dimensions of the rabbit eyes, the sample length was reduced by 50% to 0.5 cm (typical implant weight including suture: ~2.3 mg). The implants were sealed in gas-permeable bags and sterilized with ethylene oxide gas for 14 h (Anprolene Automatic Ventilated Sterilizer, Anderson Products, Chapel Hill, NC). The bags were subsequently kept under laminar air flow for 24 h to remove any residual ethylene oxide. The implantation plan is summarized in Table III.

The rabbits were housed in separate cages. Before surgery, the animals were sedated by subcutaneous injection of ketamine and acepromazine (40–60 mg/kg and 1 mg/kg, respectively). Anesthesia was induced with isoflurane (4–5% in oxygen) in an induction chamber and maintained at 2–3% during the surgery using a respirator system. To reduce ocular infections, the rabbits received antibiotic eye drops preoperatively and postoperatively. The animals were prepped and draped in a standard fashion using three drops of Zymar[®] antibiotic drops in the *cul-de-sac* of each eye, spaced 5 min apart, followed by 5% betadine solution being placed in the eye and a sterile drape around the eye. Each rabbit received only one implant per eye, which was placed either intrasclerally or intravitreally (Table III). The eye and the site of implantation were randomized. Per rabbit, either BaSO₄-loaded or plain PPF/PVP implants were used. The total number of rabbits was four. For intrascleral implantation, the conjunctiva was opened from the limbus superior-temporally using Wescott scissors. A 20-gauge needle or a crescent blade was used to create a partial thickness epi-scleral/sub-Tenon's pocket in the superior-temporal quadrant. One implant was then inserted in the pocket. The conjunctiva was closed with an interrupted 7-0 vicryl suture. Topical Maxitrol[®] ointment was placed at the end of the case. To place the intravitreal implants, the conjunctiva was opened 4 mm from the limbus superior-temporally

using Wescott scissors. A 20-gauge microvitreous blade was used to create a full thickness stab incision, 4 mm from the limbus, in the superior-nasal quadrant through which the implant was inserted into the vitreous cavity. The suture, imbedded in the implant, was cut short and left under the conjunctiva. A 7-0 vicryl suture was used to close the wound and insure a watertight closure. The conjunctiva was closed with an interrupted vicryl suture, and topical Maxitrol[®] ointment was applied.

Two weeks postimplantation, the rabbits were euthanized with an overdose of potassium chloride (KCl) (0.485 mg/kg body weight). Before enucleation, the anterior chamber was examined under direct illumination, and the posterior segment was examined with an indirect ophthalmoscope, the standard technique for both human and animal examinations. Fundus photographs were taken using a conventional hand-held fundus camera (Handheld Non-Mydriatic Fundus Camera NM-200D, Nidek, Japan). These examinations, which were also performed before implantation, revealed no pathogenic findings in response to the implant placement and no indications of compromised vision.

Specimen preparation and histology

All enucleated globes were immediately fixed in a 1:1 mixture of 10% neutral buffered formalin (Sigma-Aldrich) and 1% aqueous glutaraldehyde. After 24 h, a 1 cm × 1 cm tissue square containing the intrascleral implant was resected and placed into the fixation buffer for an additional 5 h. Thereafter, the specimen was dehydrated in a graded series of alcohol and embedded in paraffin. By means of a microtome (Leica RM 2165, Leica Microsystems, Nussloch, Germany), transverse sections (5 μm thickness) were taken from the intrascleral implant and the surrounding tissue along the length of the implant. The histological sections were deparaffinized and stained with hematoxylin and eosin (H&E) for evaluation by light microscopy (Leica Microsystems, Nussloch, Germany).¹⁹ The obtained specimen was described precisely, and a semiquantitative scoring analysis of the tissue response was performed.²⁰ The soft tissue response to the intrascleral implants was scored based on the number of fibroblast layers that were found in the dense interface zone in direct contact with the implant and the looser reaction zone (capsule) between host tissue and interface zone (Table IV). For each sample, six histological slides (distributed over the implant length of 0.5 cm) were analyzed in three positions each (position 1: closest to conjunctiva, position 3: closest to retina, position 2: perpendicular to the implant axis between positions 1 and 3) (positions are illustrated in Fig. 9). The histological sections were blinded and scored randomly.

The intravitreal implants were retrieved after 3 h of fixation by dissection of the globes. The explants were washed in PBS to remove the adherent collagenous vitreous body, gently patted dry, lyophilized, and finally subjected to micro-CT analysis.

Statistics

Unless otherwise stated, all experiments were conducted in triplicate, and the results are reported as means ± SD.

TABLE IV
Histological Grading Scale as Used for Explant Analysis

Score	Interface Zone, Semiquantitatively	Reaction Zone (Capsule), Semiquantitatively
4	1–2 cell layers	1–4 cell layers
3	3–6 cell layers	5–9 cell layers
2	7–20 cell layers	10–20 cell layers
1	>20 cell layers	>20 cell layers
0	Not applicable/ cannot be evaluated	Not applicable/ cannot be evaluated

The number of fibroblast layers at the interface zone and the reaction zone (capsule) (Fig. 9) were counted and used to semiquantitatively score the tissue response.

Single-factor analysis of variance was used in conjunction with a multiple comparison test (Tukey's test) to assess statistical significance ($p < 0.05$ unless otherwise stated).

RESULTS AND DISCUSSION

Ophthalmic drug release from photocrosslinked PPF/PVP drug-delivery systems

Promising results on long-term release of the antiinflammatory corticosteroid FA from photocrosslinked PPF/PVP matrices designed for ophthalmic applications have encouraged further investigation of such matrices for the controlled delivery of other ophthalmic drugs.⁶ Matrices composed of three parts PPF and two parts NVP were loaded with different amounts of the ophthalmic drugs AZ, DP, and TM and crosslinked through a blue light in the presence of the photoinitiator BAPO. Because of different solubilities of the drugs in NVP, the maximum loading achieved was 10% (w/w) for DP and 5% (w/w) for AZ (Table I). To investigate the effects of drug loading on release kinetics, matrices incorporating half the drug load were fabricated. The drug TM was encapsulated at a concentration of 5% (w/w) to allow for the comparison of release kinetics between all the three drugs at a loading of 5%. In comparison to FA, which is a lipophilic drug that does not dissociate in aqueous buffers and is poorly water soluble, the model drugs chosen for this study dissociate in physiological buffer and are thus characterized by higher water solubilities. Chemically, AZ and DP are sulfonamides with pK_a values of 7.2 and 7.4, respectively (Fig. 1). The sulfonamide functionality dissociates in aqueous solutions of physiological pH to a considerable extent. TM is the maleic acid salt of the basic drug timolol and therefore well soluble in water and physiological buffers. A relative prediction of the diffusion rates in the crosslinked matrices, however, appears difficult because in addition to degree of dissociation, the drugs also differ in MW. No reliable

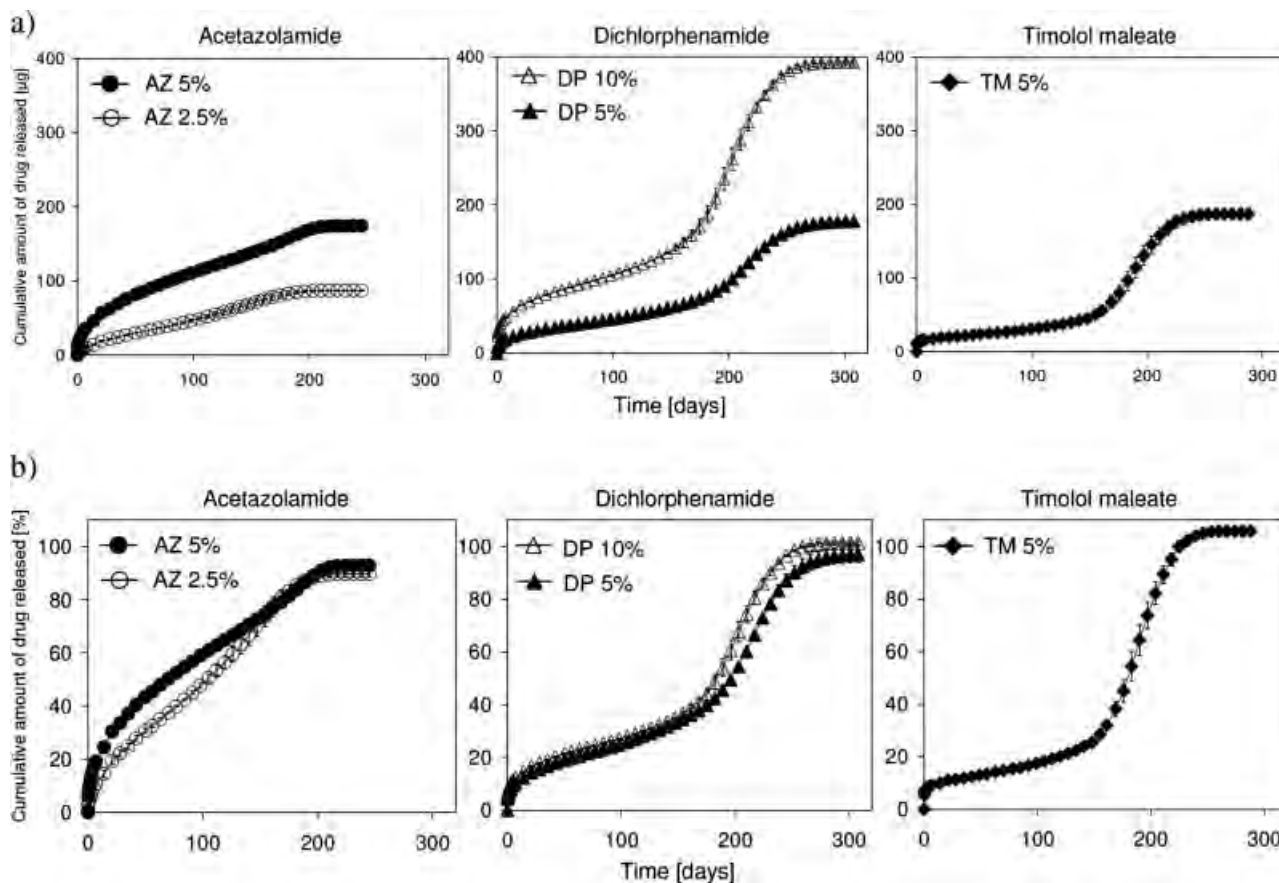


Figure 2. (a) Absolute (μg) and (b) relative (%) cumulative amounts of acetazolamide (AZ), dichlorphenamide (DP), and timolol maleate (TM) released from photocrosslinked PPF/PVP matrices of different composition (Table I): (○) AZ 2.5%, (●) AZ 5%, (▲) DP 5%, (△) DP 10%, and (◆) TM 5%. Data represent means \pm SD for $n = 3$.

comparison of drug solubility in water or buffer is possible based on literature data because of discrepancies in experimental conditions between different data sources. During HPLC studies, we have determined solubilities of 0.03 mg/mL and 0.93 mg/mL for FA and DP, respectively, in PBS at 37°C. AZ and TM both showed solubility values higher than 1 mg/mL under the same conditions. Despite these differences in solubility and hydrophilicity, the AZ-, DP-, and TM-loaded matrices displayed a sustained long-term drug release (Fig. 2). Regardless of loading dose, the matrices were found depleted of AZ after 245 days, while the third data point without DP release was detected after 308 days and after 287 days for TM. The time points at which 99% of the total amount of released drug were reached are the following: 207 days (AZ 2.5%), 220 days (AZ 5%), 280 days (DP 5%), 266 days (DP 10%), and 253 days (TM 5%). The release profiles displayed a bimodal profile with a secondary burst at approximately day 160. This burst was least pronounced for the AZ-loaded matrices, which is attributed to the almost complete depletion of drug at this time point. Secondary burst effects are known for biodegradable formulations, and the

burst is attributed to polymer degradation and/or erosion and the corresponding increase in theoretical mesh size that accelerates drug diffusion within the matrices.^{6,21,22} In more detail, the cumulative release profiles for each drug can be divided into four phases. After the initial burst release, the drug release tapered down over the first week. During a subsequent period of several weeks (AZ until day 168, DP until day 154, TM until day 147), the drug was released almost linearly from all systems. During the next release period, the drug release was accelerated, and the release rates increased steadily until maximum release was reached between days 190 and 225. Thereafter, the release rates gradually decreased, indicating the fourth and final release phase, until drug release was terminated (AZ: 245 days, DP: 315 days, and TM: 287 days). At termination of the release studies (t_{end}), the different formulations had released their drug load completely (AZ 5%: $92.8\% \pm 0.5\%$, DP 5%: $97.1\% \pm 3.2\%$, and TM 5%: $105.8\% \pm 1.8\%$) (Fig. 2). Comparison of absolute and cumulative release profiles from formulations loaded with different amounts of the same drug revealed different effects of drug loading. Increased AZ loading resulted

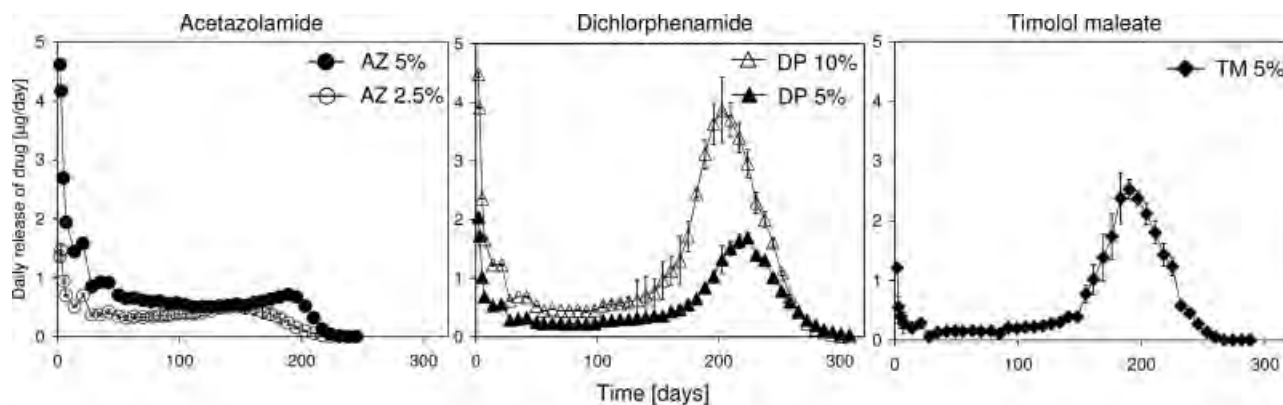


Figure 3. Drug release rates (expressed as microgram drug per day) calculated for the different drugs from the *in vitro* release data. (○) AZ 2.5%, (●) AZ 5%, (▲) DP 5%, (Δ) DP 10%, and (◆) TM 5%. Data represent means \pm SD for $n = 3$.

in elevated absolute and relative release profiles, indicating that maximum solubility concentration was not reached in AZ 2.5% samples and that water uptake and drug dissolution followed a faster kinetic than drug diffusion. Consequently, in samples containing 5% AZ, higher concentrations of dissolved AZ could be reached per unit volume, and the diffusional pressure was increased, which resulted in an accelerated diffusion-controlled drug release. For DP-loaded samples, absolute drug release increased with drug loading, but the relative release profiles were almost identical. This indicates that during the period of diffusion-controlled drug release, exactly double the amount of drug was released from DP 10% than from DP 5%. Consequently, this behavior was also not controlled by limited drug solubility but by the kinetics of water uptake. If one assumes that water penetration is the rate limiting step and initially follows zero-order kinetics, the drug will only dissolve in the hydrated volume units and diffuse out of the matrix. Because each volume unit contained double the amount of drug, the flux was doubled and the concentration gradient could not build up further due to limited water uptake.

The calculated average daily drug release rates summarized in Figure 3 also display the different release phases. After the initial burst release, the release rates stabilized over a period of ~ 2 weeks. Thereafter, the drugs were released at almost constant rates for more than 100 days. During this period, the rates ranged around 0.6 ± 0.1 $\mu\text{g}/\text{day}$ (AZ 5%), 0.3 ± 0.1 $\mu\text{g}/\text{day}$ (DP 5%), and 0.2 ± 0.1 $\mu\text{g}/\text{day}$ (TM 5%). During the third release period, the release rate increased, especially for the DP and TM-loaded formulations due to matrix degradation. Excluding the burst release, a maximum daily release of 1.7 ± 0.2 $\mu\text{g}/\text{day}$ was determined for DP 5% (day 224) and 2.5 ± 0.2 $\mu\text{g}/\text{day}$ for TM 5% (day 190). The highest peak release rate was 3.9 ± 0.1 $\mu\text{g}/\text{day}$ and determined for

DP 10% at day 203 (Fig. 3). Drug release from AZ 5% only increased to 0.7 ± 0.0 $\mu\text{g}/\text{day}$ (day 189). A discussion of these values is difficult because very limited information is available on therapeutic drug levels (especially for delivery to the posterior chamber of the eye) for the selected model drugs. An effective concentration for AZ in the aqueous humor (anterior chamber) has been reported as 0.276 ± 0.071 $\mu\text{g}/\text{mL}$ in rabbit eyes.²³ Considering a volume of a few hundred microliters for the aqueous humor, the release rates appear to cover a suitable range to reach effective concentrations.²⁴ If needed, strategies to elevate the release rates and eliminate the secondary burst, for example, the use of hydrophilic release modifiers, are available and effective for PPF/PVP matrices.²⁵ Comparison of the amounts of drug released during the first 24 h (burst release) revealed a statistically significant increase in burst release for AZ 5% ($9.6\% \pm 0.4\%$) when compared to DP 5% and TM 5% (Fig. 4). DP 5% showed the lowest burst release ($6.3\% \pm 0.4\%$) and the amount released from TM 5% was only slightly higher ($7.4\% \pm 0.8\%$). Based on those data and considering the small burst release values that had been found for FA,⁶ the burst release seemed to correlate mainly with substance solubility. Within formulations loaded with the same drug, the relative burst release from the highly loaded sample exceeded the burst found for the formulation with half the drug load. These findings are in accordance with the results of the FA release experiments.⁶ In general, the burst release from all tested formulations was moderate and ranged between 6 and 10%.

Comparison of drug release kinetics and drug partition profiles

Characteristic parameters were derived from the obtained release profiles of the 5% drug samples and

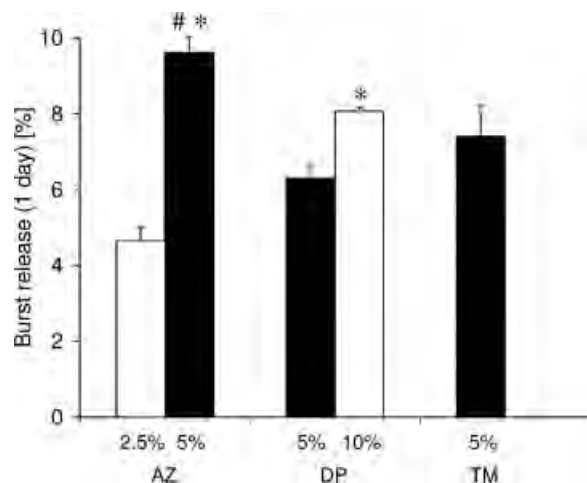


Figure 4. Relative, cumulative amount of drug released within the first day (burst release) from photocrosslinked PPF/PVP matrices loaded with different drugs. Columns and error bars represent means \pm SD for $n = 3$. Statistically significant ($p < 0.01$) differences in burst release between samples with 5% drug loading are indicated by #. Statistically significant ($p < 0.01$) differences in burst release between different loadings of the same drug are denoted by *.

summarized in Figure 5(a) to enable the comparison of the data sets. The release kinetics were characterized by the times after which 20% ($t_{20\%}$), 50% ($t_{50\%}$), and 90% ($t_{90\%}$) of the theoretical drug load was released from the matrices. The amount of drug that was released from each formulation after 20 weeks was expressed as $m_{20\text{weeks}}$. This time point was chosen because it approximately denotes the end of the release period during which the drug release was predominantly controlled by diffusion. Thereafter, the drug release was accelerated by polymer degradation and/or erosion and the release kinetics became more complex. Accordingly, only the time point $t_{20\%}$ fell into the period of diffusion-controlled drug release in all formulations (Fig. 2). $t_{50\%}$ and $t_{90\%}$ were reached in the period of accelerated drug release. Data from a previous release study with FA were added, and the characteristic parameters were determined for formulation FA 5% (PPF/NVP = 3/2).⁶ The PPF macromer used in this study was identical to the one used for the AZ and DP-loaded matrices (Table I). Comparison of $t_{20\%}$ and $m_{20\text{weeks}}$ revealed the following information on drug release kinetics [Fig. 5(a)]. The fastest drug release was observed for AZ 5%, followed by DP 5% and TM 5%, and FA was the drug that was released slowest. $t_{50\%}$ and $t_{90\%}$ showed a similar trend with the exception that TM release was accelerated faster than the release of DP. This might be correlated with the finding that water uptake into DP-loaded formulations was rate limiting during diffusion-controlled drug release. Drug release from DP-loaded

samples was strongly accelerated at the point when polymer degradation allowed for increased water uptake. Formulations loaded with AZ and TM, the drugs with the highest solubility in this study, might have attracted the release buffer more constantly over the course of the release study. $t_{90\%}$ for FA 5% could not be determined because the release study was stopped after 57 weeks, and, at that time, the cumulative drug release from formulation FA 5% (PPF/NVP = 3/2) had just reached 50% of its original loading.⁶

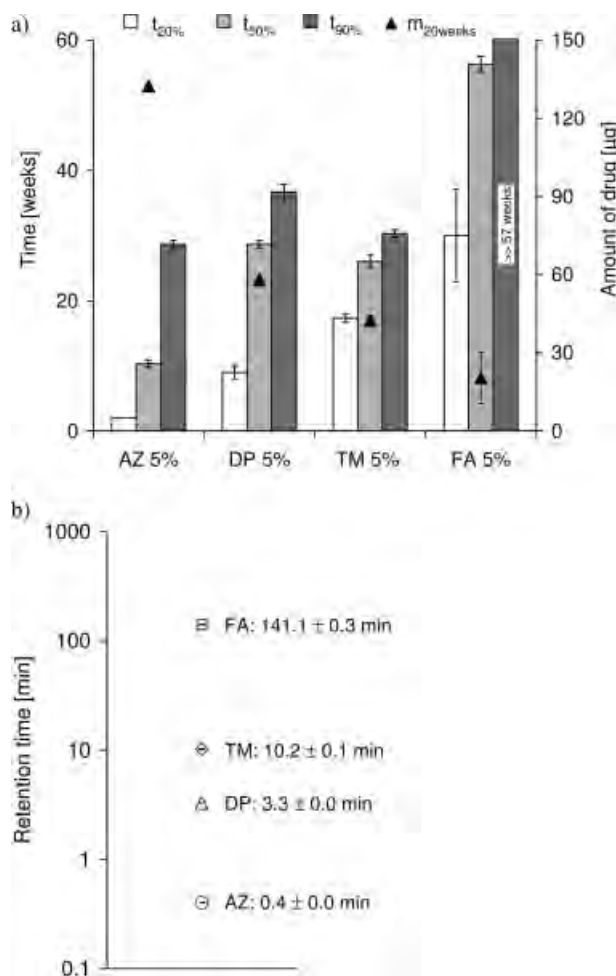


Figure 5. Correlation between drug elution profiles and release kinetics. (a) Kinetic information ($t_{50\%}$, $t_{90\%}$, and $m_{20\text{weeks}}$) on the release of acetazolamide (AZ), dichlorphenamide (DP), and timolol maleate (TM) as determined from the release data of AZ 5%, DP 5%, and TM 5% samples. Information for fluocinolone acetonide (FA) was calculated from previously published data.⁶ $t_{50\%}$ and $t_{90\%}$ denote the time in weeks after which 50% and 90% of the drugs was released. $m_{20\text{weeks}}$ represents the mass of drug that was released after 20 weeks. (b) Absolute retention times (RTs) of the investigated drug dissociated in phosphate buffered saline at 37°C (release buffer) on a reversed-phase column. Fluocinolone acetonide (FA) was analyzed together with acetazolamide (AZ), dichlorphenamide (DP), and timolol maleate (TM) for comparison.

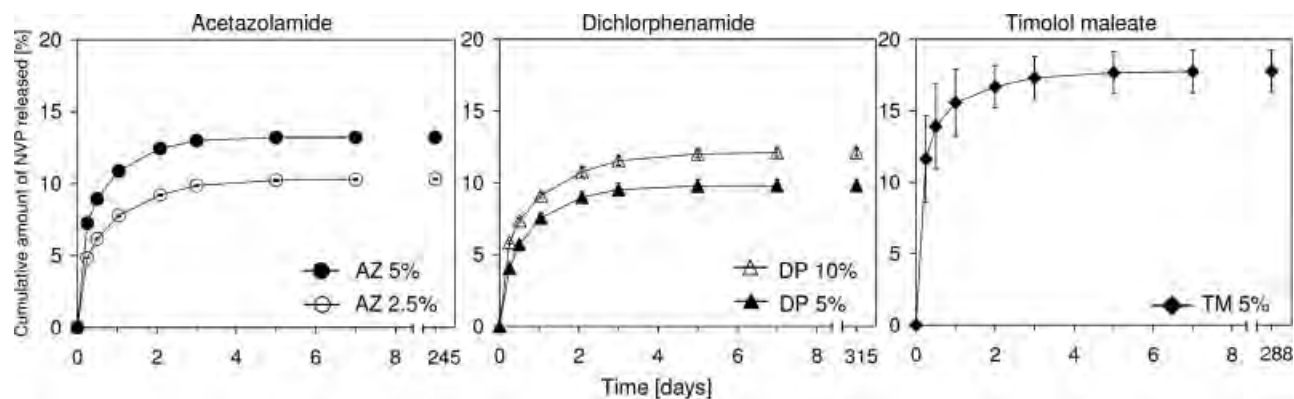


Figure 6. Relative cumulative amounts of residual *N*-vinyl pyrrolidone (NVP) released from photocrosslinked PPF/PVP matrices of different composition (Table I): (○) AZ 2.5%, (●) AZ 5%, (▲) DP 5%, (Δ) DP 10%, and (◆) TM 5%. Data represent means \pm SD for $n = 3$.

The kinetic parameters that compared diffusion-controlled drug release indicated that the drugs were released in the following order: AZ \gg DP > TM \gg FA. Accordingly, TM, which was the only salt among the investigated drugs, was not released following the fastest kinetics. Drug solubility data would have designated DP and FA as the drugs with the slowest release kinetics. A quick tool that could allow for the estimation of drug partition in any dissociated state between an aqueous phase and a stationary hydrophobic polymer phase is reversed-phase liquid chromatography. The investigated drugs were dissolved in PBS (pH 7.4) to equilibrate drug dissociation. The drug-PBS solutions were injected on a C8 reversed-phase column, separated at 37°C and eluted by a PBS-acetonitrile mixture (85:15 (v/v)) as mobile phase on a HPLC system equipped with UV detection. From the chromatograms, the absolute RTs of the drugs were calculated and compared [Fig. 5(b)]. The absolute RTs are influenced by drug dissociation, hydrophilicity, and MW, and thus enable a relative comparison of the drug with regard to these parameters. The order in which the drugs were eluted correlated well with the kinetic properties that were determined from the *in vitro* release study. AZ showed only minor interactions with the hydrophobic column ($RT_{AZ} = 0.4$ min). The RTs of DP and TM ranged within the same order of magnitude and by far the longest retention was determined for FA [Fig. 5(b)]. The drugs were eluted in the same order when the experiment was repeated on a more hydrophobic, C18 reversed-phase column in combination with a PBS-acetonitrile gradient, which was necessary to elute the more hydrophobic drugs, especially FA (data not shown). Altogether, the relative comparison of elution profiles on reversed-phased columns appears to be a suitable method to relatively compare the drug properties relevant for diffusion-controlled drug release from hydrophobic polymer matrices.

NVP release from photocrosslinked PPF/PVP drug-delivery systems

The amount of residual NVP monomers released from the photocrosslinked polymer matrices was also determined by HPLC and is summarized in Figure 6. TM-loaded systems showed the highest absolute (231.0 ± 28.6 μ g) and relative release of NVP monomers ($17.8\% \pm 1.5\%$ with respect to the theoretical amount of NVP monomers) over the course of 287 days. Matrices loaded with 5% AZ released $13.2\% \pm 0.1\%$ of NVP monomers, followed by DP 5% ($9.8\% \pm 0.4\%$). For each tested formulation, more than 90% of the total amount of residual NVP monomers detected were released from the matrices within the first 7 days; more than 80% were released within the first 2 days from all tested formulations. The amounts of released NVP correlated with the UV-absorbance wavelength of the drugs and with the drug load within groups loaded with the same drug. TM-loaded matrices released the highest amounts of NVP, and the absorbance maxima of TM (295 nm) was closest to the peak wavelength of the blue light lamp (470 nm) used for photocrosslinking. Formulations loaded with DP, which best absorbs UV light at 232 nm, released the lowest amounts of unreacted NVP. The NVP release from samples containing AZ (265 nm) ranged in between. With regard to matrix fabrication, during which all samples were exposed to blue light for equal amounts of time, it appears likely that the drugs with absorption maxima at higher wavelengths absorbed more of the applied photoenergy, which resulted in a less complete cross-copolymerization of the matrix components and an increased NVP release. Similarly, one can explain the higher amounts of NVP that were released from the highly loaded formulations (AZ 5% and DP 10%) when compared with the samples loaded with half the amounts of drug (AZ 2.5% and DP 5%). In general, the presence

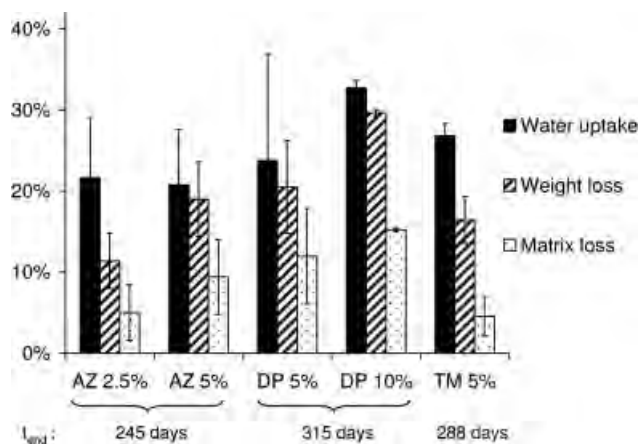


Figure 7. Water uptake, weight loss, and matrix loss of the different drug-loaded PPF/PVP matrices as determined by gravimetric analysis. Columns and error bars represent means \pm SD for $n = 3$.

of residual NVP monomers in the photocrosslinked delivery devices could be a possible safety concern.²⁶ For that reason, a maximum of 0.2% (w/w) NVP monomers is tolerated in PVP for pharmaceutical applications by the United States Pharmacopoeia (USP).²⁷ If this limit is applied to the formulations investigated here, the critical amount of NVP is released within the first 3 days. The cumulative amount of NVP released after day 3 until the termination of drug release was clearly below the critical limit of 0.2% in all formulations. A 3-day extraction treatment of the samples before application would be an effective strategy to yield devices that would meet this specific requirement of the USP. At the same time, the burst release of the samples would be reduced, and a more constant drug release could be obtained during the first days of drug release after implantation.

Gravimetric analysis

Gravimetric analysis of the polymeric release devices revealed comparable water uptake values for all tested formulations, especially with regard to the 5% (w/w) drug-loaded systems (Fig. 7). The values ranged between 20.8% \pm 6.8% for AZ 5% and 26.8% \pm 3.2% for TM 5%. The highest water uptake was found for DP 10% with 32.7% \pm 0.9%. For mass loss and matrix loss, the lowest values were found for AZ 2.5% and TM 5%, respectively. When AZ and DP-loaded formulations, which are all based on the same PPF macromer, are compared, it can be concluded that drug loading and exposure time to release buffer have a positive effect on matrix swelling and erosion. A higher drug load created more void space upon drug release that was filled with release buffer and yielded higher matrix water content. As a conse-

quence of the increased water content, polymer chain degradation and matrix erosion were favored. Overall, 5–15% polymer erosion was found for the investigated formulations, which indicates hydrolytic degradation of the photocrosslinked PPF/PVP matrices. Consequently, one can assume that the secondary burst in drug release was associated with polymer degradation and matrix erosion. Matrix loss in TM 5% samples was lower than for AZ 5% and DP 5%. Although the TM-loaded samples were fabricated from a different PPF macromer, the effect of the MW differences of the macromers on matrix degradation is negligible.¹⁴ The different degradation profiles are more likely an effect of the basicity of TM. The pK_a of TM is 9.2, classifying it as a weak base. AZ and DP are characterized as weak acids with pK_a values of 7.2 and 7.4, respectively. It has been shown that the erosion of polyester-type biodegradable polymers can be decelerated by the incorporation of basic drugs.²⁸

Matrix morphology of the PPF/PVP drug-delivery systems

Micro-CT imaging of the drug-loaded photocrosslinked PPF/PVP matrices prior and subsequent to the *in vitro* release study revealed a homogenous appearance without visible pores after fabrication and at t_{end} (data not shown). The results were similar to those obtained for FA-loaded matrices.⁶ The structural integrity of all tested formulations was maintained over the course of the release study. Image analysis of a 1.5-mm long representative segment of the different samples was used to quantify any changes in cross-sectional area of the polymer rods over the investigated release periods. A comparison of the average cross-sectional areas instead of the mean sample diameters appeared more appropriate because of the imperfect cylindrical shape of some specimens. A decrease in cross-sectional area was found for all investigated formulations (Fig. 8). For AZ and DP-loaded samples, the trends in cross-sectional area change correlated with the matrix loss data determined by gravimetric analysis (Fig. 7). The differences in sample area became more prominent with increased drug loadings and exposure times to release buffer (Fig. 8). Sample TM 5%, which was fabricated from a different PPF macromer and showed the lowest matrix loss values, however, exhibited the largest relative area decrease of all formulations. As mentioned earlier, the basicity of TM might determine the observed difference in matrix degradation of the TM-loaded samples when compared to the matrices loaded with the acidic sulfonamides AZ and DP. The potential of TM to buffer acidic degradation products in the polymer bulk and suppress autocatalysis might have caused stronger degradation in the perimeter of

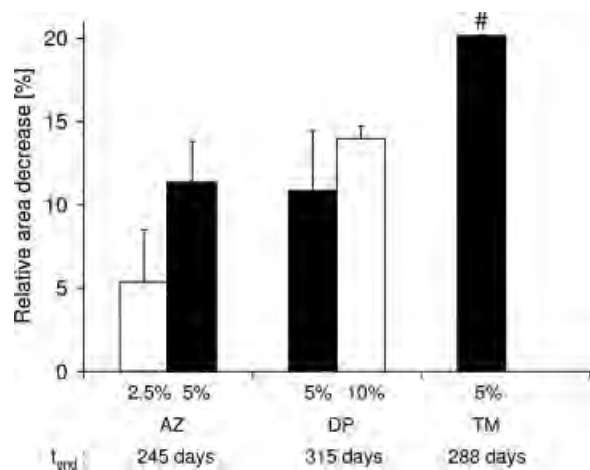


Figure 8. Relative decrease in average cross-sectional area of the drug delivery systems (Table I) during the *in vitro* release study as determined by micro-CT imaging. Columns and error bars represent means + SD for $n = 3$. Statistically significant ($p < 0.05$) differences between samples with 5% drug loading are indicated by #.

the rod as compared to the bulk. This could have caused an increased volume loss in combination with a moderate mass loss.

Rabbit implantation study

The encouraging results of the *in vitro* release study motivated a preliminary implantation study to assess the feasibility of the polymer rods for intraocular application and to determine the soft tissue response to the material. Samples were implanted either into a pocket between the episclera and sclera or directly into the vitreous humor as summarized in Table III. No handling problems with the implants occurred during surgery, and all implants were successfully placed into the target structures. Eye examinations in combination with fundus photographs that were conducted immediately before the implantation surgery and at the end of the 2-week study revealed no pathogenic developments and no signs of impaired vision or vision loss. Three of four intrascleral implants (1S-, 2S+, and 3S+) could be resected with the surrounding tissue and processed for analysis. The fourth implant was found to have slipped out of the tissue pocket but still sutured to the conjunctiva after enucleation. After fixation, the specimens were scanned with micro-CT and analyzed histologically. Figure 9(a) is a gross view of a representative H&E stained cross-section through specimen 1S-. In general, the implants maintained their structural integrity and appeared transparent, while the surrounding tissue stained blue and pink. The implant was positioned between the episclera and sclera as attempted, and both sclera and retina were not affected by the

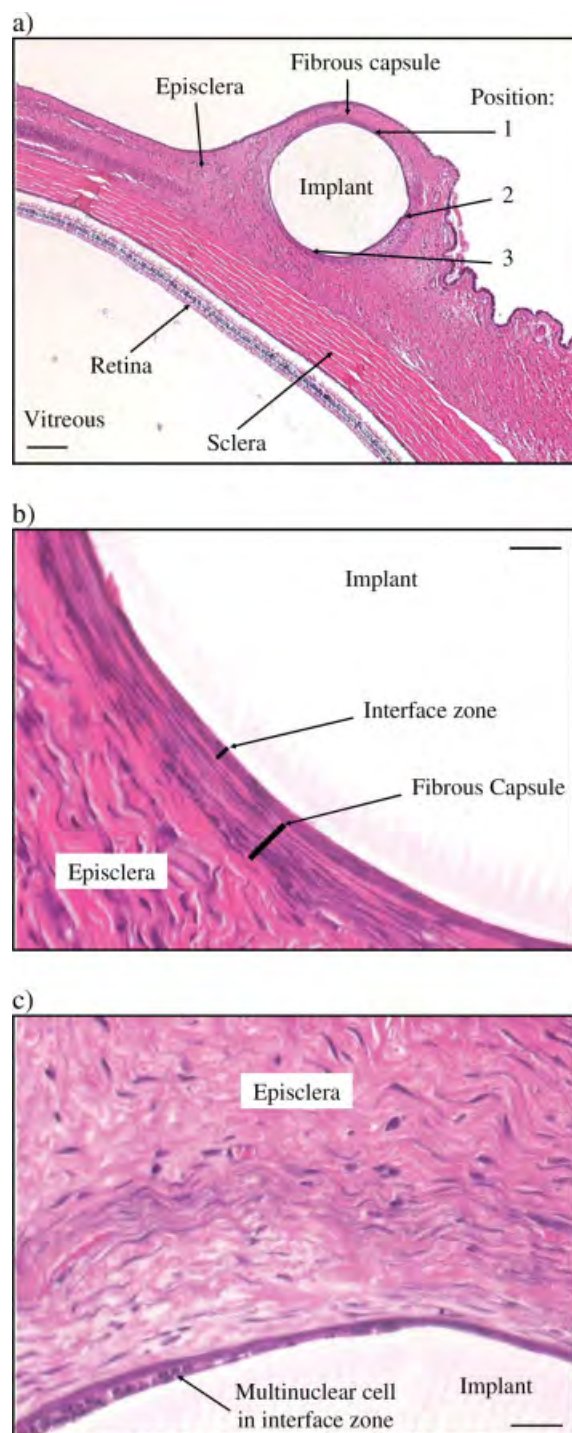


Figure 9. Representative histological sections of the implant-tissue interface of intrascleral implants after 2 weeks of implantation. (a) Gross view of an intrascleral implant. The implant appears colorless in all images. A uniform thin fibrous capsule was found at the perimeter of the implant. Numbers 1–3 indicate the positions at which the different zones were scored. Scale bar represents 200 μm , original magnification was 4 \times . (b) Close-up of the implant-tissue interface depicting the interface zone and the retention zone (capsule). (c) Close-up of a implant-tissue interface at which a small number of multinuclear cells were observed. Scale bars in (b) and (c) represent 25 μm , and the original magnification was 40 \times . [Color figure can be viewed in the online issue, which is available at www.interscience.wiley.com.]

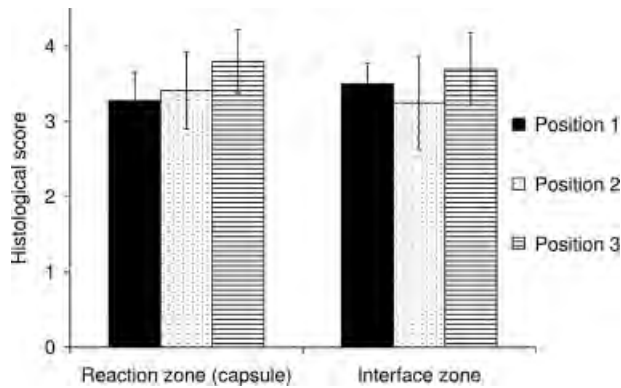


Figure 10. Histological scores determined for the interface and the reaction zones of intrascleral implants at three positions [Fig. 9(a)]. Columns and error bars represent mean \pm SD of the scores for implants 1S-, 2S+, and 3S+. The score for each sample was averaged from six different slides.

implant [Fig. 9(a)]. For all intrascleral implants, the formation of a small fibrous capsule was observed [Fig. 9(a,b)]. The soft tissue response was evaluated semiquantitatively by counting the number of fibroblast layers that constitute the dense interface and the looser reaction zone (fibrous capsule) [Fig. 9(b)] in three positions [Fig. 9(a)] of six cross-sections distributed equally along the implant. In a few sections, a limited number of multinuclear cells were found in the interface zone [Fig. 9(c)]. Based on the number of fibroblast layers, a histological score was determined (Table IV). Similar scoring systems have been widely used to analyze a biomaterial-tissue response.^{20,29} Figure 10 summarizes the results of the histological scoring of the tissue response to the intrascleral implants. No significant difference was found between the plain and the barium sulfate-loaded samples, and a mean score was calculated from the individual scores of the three explants. A mild tissue response was observed in all three positions, and scores above

three were reached for the interface and reaction zone (Fig. 10). The presence of inflammatory cells and macrophages at the implant-tissue interface was scarce. Considering the early time point (2 weeks), the low abundance of such cells is a very promising finding with regard to implant biocompatibility. Altogether, the implants were well tolerated and caused a low inflammatory response. In good accordance with the *in vitro* results, no accelerated implant degradation was visible after 2 weeks. No further information could be obtained from the micro-CT analysis because the contrast between polymer implant and surrounding tissue was insufficient, even for the barium sulfate-loaded samples, to clearly threshold and reconstruct the implant for dimensional analysis [Fig. 11(a)]. A more extensive *in vivo* study will be necessary to confirm these results. The surgical procedure and implant dimensions in this study provided a suitable model for the evaluation of intraocular compatibility and can be adapted for future studies.

Similar conclusions can be drawn for the intravitreal implants. In all cases, no signs of an inflammatory response became apparent. Micro-CT imaging of the explants revealed structural integrity of the implants, and no pore formation was visible after 2 weeks *in vivo* [Fig. 11(b,c)]. From past *in vivo* experience with PPF-based implants and the results of the *in vitro* release study, no significant degradation is expected over a period of 2 weeks. Dimensional analysis of the explants confirmed this expectation (data not shown).

CONCLUSIONS

This study investigated the potential application of monolithic, nonporous, photocrosslinked PPF/PVP matrices as ophthalmic drug-delivery systems. Three

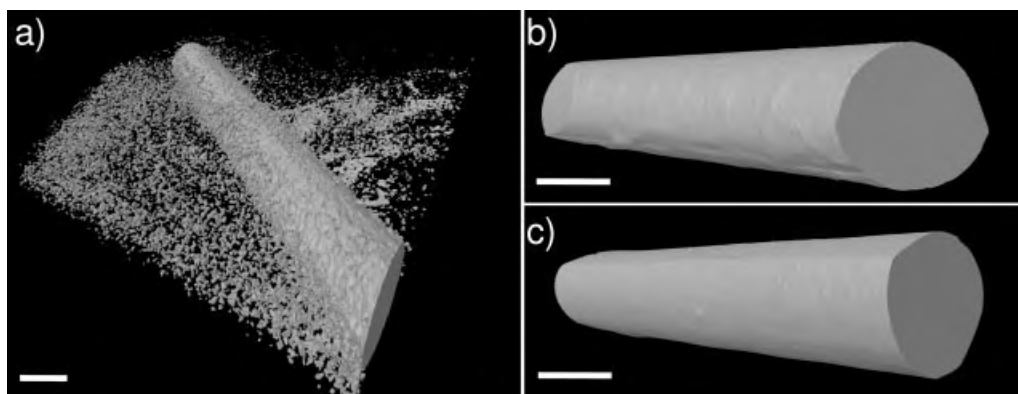


Figure 11. Representative 3-D micro-CT reconstructions of photocrosslinked PPF/PVP matrices from the rabbit implantation study. (a) Barium sulfate-loaded matrix (implant 3S+) as retrieved with surrounding scleral tissue after intrascleral implantation for 14 days. Scale bar represents 0.5 mm. (b) Plain matrix (implant 4V-) before intravitreal implantation and (c) after explantation and processing. Scale bars indicate 0.25 mm.

model drugs were chosen that dissociate to different extents in aqueous media and exhibit considerable water solubility. Despite their hydrophilicity, all three drugs were released from the photocrosslinked PPF-based matrices in a well-sustained manner over periods between 200 and 300 days. The release kinetics of the different drugs was controlled by diffusion and matrix bulk erosion. Diffusion-controlled drug release was found to qualitatively correlate with physicochemical properties of the drugs. Gravimetric analysis and micro-CT imaging revealed polymer degradation associated with mass loss and a decrease in matrix cross-sectional area. A 2-week rabbit *in vivo* study evaluated the soft tissue response to drug-free implants after intrascleral and intravitreal application. Histological evaluation revealed minimal fibrous capsule formation and no signs of a significant inflammatory response to the implanted biomaterial. Overall, the results of both the *in vitro* release study and the *in vivo* tissue response study were very promising and indicate that the photocrosslinked PPF-based matrices are versatile drug-delivery devices allowing for the long-term delivery of a variety of ophthalmic drugs with different physicochemical properties.

The authors acknowledge the expert guidance of Ms. Tiffany Sheffield-Lopez and Dr. Katherine C. Ambrose (University of Texas Health Science Center, UTMB, Houston, TX) regarding the tissue sample preparation and histology.

References

- Cunha-Vaz JG. The blood-retinal barriers system. Basic concepts and clinical evaluation. *Exp Eye Res* 2004;78:715–721.
- Peyman GA, Ganiban GJ. Delivery systems for intraocular routes. *Adv Drug Deliv Rev* 1995;16:107–123.
- Colthurst MJ, Williams RL, Hiscott PS, Grierson I. Biomaterials used in the posterior segment of the eye. *Biomaterials* 2000;21:649–665.
- Yasukawa T, Ogura Y, Tabata Y, Kimura H, Wiedemann P, Honda Y. Drug delivery systems for vitreoretinal diseases. *Prog Retin Eye Res* 2004;23:253–281.
- Geroski DH, Edelhauser HF. Transscleral drug delivery for posterior segment disease. *Adv Drug Deliv Rev* 2001;52:37–48.
- Haesslein A, Ueda H, Hacker MC, Jo S, Ammon DM, Borazjani RN, Kunzler JF, Salamone JC, Mikos AG. Long-term release of fluocinolone acetonide using biodegradable fumarate-based polymers. *J Control Release* 2006;114:251–260.
- Ueda H, Hacker MC, Haesslein A, Jo S, Ammon DM, Borazjani RN, Kunzler JF, Salamone JC, Mikos AG. Injectable in situ forming poly(propylene fumarate)-based ocular drug delivery systems. *J Biomed Mater Res A* 2007;83:656–666.
- Kaur IP, Smitha R, Aggarwal D, Kapil M. Acetazolamide: Future perspective in topical glaucoma therapeutics. *Int J Pharm* 2002;248:1–14.
- Ashburn FS, Gillespie JE, Kass MA, Becker B. Timolol plus maximum tolerated antiglaucoma therapy: A one-year followup study. *Surv Ophthalmol* 1979;23:389–394.
- Lindsog S. Structure and mechanism of carbonic anhydrase. *Pharmacol Ther* 1997;74:1–20.
- Bourges JL, Bloquel C, Thomas A, Froussart F, Bochot A, Azan F, Gurny R, BenEzra D, Behar-Cohen F. Intraocular implants for extended drug delivery: Therapeutic applications. *Adv Drug Deliv Rev* 2006;58:1182–1202.
- Wang Y, Challa P, Epstein DL, Yuan F. Controlled release of ethacrynic acid from poly(lactide-co-glycolide) films for glaucoma treatment. *Biomaterials* 2004;25:4279–4285.
- Maurice DM. Drug delivery to the posterior segment from drops. *Surv Ophthalmol* 2002;47:S41–S52.
- Haesslein A, Hacker MC, Mikos AG. Effect of macromer molecular weight on in vitro ophthalmic drug release from photo-crosslinked matrices. *Acta Biomater* 2008;4:1–10.
- Shung AK, Timmer MD, Jo S, Engel PS, Mikos AG. Kinetics of poly(propylene fumarate) synthesis by step polymerization of diethyl fumarate and propylene glycol using zinc chloride as a catalyst. *J Biomater Sci Polym Ed* 2002;13:95–108.
- Timmer MD, Carter C, Ambrose CG, Mikos AG. Fabrication of poly(propylene fumarate)-based orthopaedic implants by photo-crosslinking through transparent silicone molds. *Biomaterials* 2003;24:4707–4714.
- Braumann T. Determination of hydrophobic parameters by reversed-phase liquid chromatography: theory, experimental techniques, and application in studies on quantitative structure-activity relationships. *J Chromatogr A* 1986;373:191–225.
- Kaliszan R. Quantitative structure-retention relationships applied to reversed-phase high-performance liquid chromatography. *J Chromatogr A* 1993;656:417–435.
- Holland TA, Bodde EWH, Baggett LS, Tabata Y, Mikos AG, Jansen JA. Osteochondral repair in the rabbit model utilizing bilayered, degradable oligo(poly(ethylene glycol) fumarate) hydrogel scaffolds. *J Biomed Mater Res A* 2005;75:156–167.
- Jansen JA, Dhert WJA, Van der Waerden JPCM, Von Recum AF. Semi-quantitative and qualitative histologic analysis method for the evaluation of implant biocompatibility. *J Invest Surg* 1994;7:123–134.
- Wang F, Lee T, Wang CH. PEG modulated release of etanidazole from implantable PLGA/PDLA discs. *Biomaterials* 2002;23:3555–3566.
- Siepmann J, Gopferich A. Mathematical modeling of bioerodible, polymeric drug delivery systems. *Adv Drug Deliv Rev* 2001;48:229–247.
- Aggarwal D, Pal D, Mitra AK, Kaur IP. Study of the extent of ocular absorption of acetazolamide from a developed niosomal formulation, by microdialysis sampling of aqueous humor. *Int J Pharm* 2007;338:21–26.
- Macknight AD, McLaughlin CW, Peart D, Purves RD, Carre DA, Civan MM. Formation of the aqueous humor. *Clin Exp Pharmacol Physiol* 2000;27:100–106.
- Haesslein A, Hacker MC, Ueda H, Ammon DM, Borazjani RN, Kunzler JF, Salamone JC, Mikos AG. Matrix modifications modulate ophthalmic drug delivery from photo-crosslinked poly(propylene fumarate)-based networks. *J Biomater Sci Polym Ed* 2008. In press.
- Klimisch H-J, Deckardt K, Gembardt C, Hildebrand B, Kuttler K, Roe FJC. Subchronic inhalation and oral toxicity of *N*-vinylpyrrolidone-2. Studies in rodents. *Food Chem Toxicol* 1997;35:1061–1074.
- Povidone. *The United States Pharmacopeia (USP 24) and National Formulary (NF 19)*, United States Pharmacopeia Convention, Rockville, MD, 2000. p 1372–1373.
- Miyajima M, Koshika A, Okada J, Kusai A, Ikeda M. The effects of drug physico-chemical properties on release from copoly(lactic/glycolic acid) matrix. *Int J Pharm* 1998;169:255–263.
- Jansen JA, de Ruijter JE, Janssen PTM, Paquay YGCJ. Histological evaluation of a biodegradable polyactive (R)/hydroxyapatite membrane. *Biomaterials* 1995;16:819–827.